mater.scichina.com link.springer.com

Published online 9 July 2020 | https://doi.org/10.1007/s40843-020-1388-1
Sci China Mater 2020, 63(11): 2358–2364

Novel superhard boron-rich nitrides under pressure

Linyan Wang[1†], Rongxin Sun[1†], Wenhui Liu[1†], Zhikang Yuan[1†], Aitor Bergara[2,3,4], Xiaowei Liang[1], Shuai Chen[1], Xiang-Feng Zhou[1], Bo Xu[1], Julong He[1], Dongli Yu[1], Guoying Gao[1*] and Yongjun Tian[1]

Boron and its compounds have attracted much attention due to their interesting and complex structures [1–4]. In particular, boron-rich compounds containing icosahedral structures have excellent properties, such as low density, high hardness, high melting point and low wear coefficient. Therefore, many boron-rich compounds have been studied in recent decades [5–15], such as $B_{13}C_2$ [8], B_4C [9,10], $B_{12}O_2$ [11], $B_{12}P_2$ [12,13], and $B_{12}As_2$ [14,15].

Regarding the B-N system, some boron-rich subnitrides were also synthesized. By heating β-B and nitrogen to the temperature range of 1479–1823 K, Condon *et al.* [16] proposed for the first time that a series of two-step reactions occur with a homogeneous reaction to form "B_6N" followed by a topochemical reaction to yield boron nitride (BN). Later, Hubert *et al.* [17] claimed a high-pressure solid-state synthesis of "B_6N" by reacting amorphous boron and hexagonal boron nitride (h-BN) at 7.5 GPa and 1700°C, which was suggested to have a structure similar to $R\bar{3}m$ B_6O. However, Solozhenko *et al.* [18] did the same experiment at the same pressure/temperature conditions and concluded that the evidence for the solid-state synthesis of B_6N with B_6O-like structure reported in Ref. [17] is inconclusive. On the other hand, Saitoh *et al.* [19] synthesized B-N films by a chemical vapor deposition containing another stoichiometry (B_4N), and the measured Raman spectra and X-ray diffraction (XRD) results revealed that the crystal structure of B_4N is similar to that of B_4C. However, the available experimental data is still insufficient to identify its accurate crystal structure and composition. Interestingly, Solozhenko *et al.* [20–23] synthesized a new boron subnitride $B_{13}N_2$ by mixing β-rhombohedral boron and h-BN at 5 GPa and 2500 K, which has the same type structure as $B_{12}O_2$ and B_4C. Moreover, Solozhenko [22] reported that $B_{13}N_2$ is a superhard material with a measured Vickers hardness of 41 GPa. However, relevant theoretical calculations suggested that $R\bar{3}m$ $B_{13}N_2$ and $R\bar{3}m$ $B_{12}N_2$ are thermodynamically unstable, and that $R\bar{3}m$ $B_{13}N_2$ was also dynamically unstable [24,25]. Alternatively, Zhang *et al.* [24] proposed another stoichiometry $B_{12.67}N_2$ (i.e., $B_{38}N_6$) constructed from a supercell of $R\bar{3}m$ $B_{13}N_2$ with a 2:1 ratio of complete N–B–N chains to boron vacancies chains, which was calculated to be both thermodynamically and dynamically stable. Moreover, a new composition $B_{38}N_6$ ($[B_{12}(N–N)]_{0.33}[B_{12}(NBN)]_{0.67}$) was predicted to be stable by Ektarawong *et al.* [25]. At the same time, another boron-rich compound, $B_{50}N_2$ (space group *P*-4*n*2; a = 8.8181(2) Å, c = 5.0427(10) Å) was synthesized under high temperature and pressure [20,23,26–29]. However, stoichiometries and crystal structures of many other boron-rich nitrides are still unclear.

In the present work, a systematic structure search for B_nN (n = 2, 3, 4, 5, 6, 8) has been performed using the CALYPSO code [30–35] with the particle swarm optimization method. Structure searches were performed in the pressure range of 0–20 GPa using models consisting of 1–8 formula units. We used the VASP code [36] with the plane-wave pseudopotential method to calculate the total energies of the structures. The Perdew-Burke-Ernzerhof (PBE) generalized gradient approximation [37] was chosen for the exchange and correlation functional and all-electron projector augmented wave (PAW) [38] pseudopotentials with $2s^22p^1$ and $2s^22p^3$ valence config-

[1] Center for High Pressure Science (CHiPS), State Key Laboratory of Metastable Materials Science and Technology, Yanshan University, Qinhuangdao 066004, China
[2] Departmento de Física de la Materia Condensada, Universidad del País Vasco, UPV/EHU, 48080 Bilbao, Spain
[3] Donostia International Physics Center (DIPC), 20018 Donostia, Spain
[4] Centro de Física de Materiales CFM, Centro Mixto CSIC-UPV/EHU, 20018 Donostia, Spain
† These authors contributed equally to this paper.
* Corresponding author (email: gaoguoying@ysu.edu.cn)

urations were adopted for B and N atoms, respectively. The plane-wave energy cutoff is 800 eV for all the structures, and the *k*-point meshs are increased until enthalpies converge to within 1 meV per atom.

We carried out a detailed structure search on B_nN (n = 2, 3, 4, 5, 6, 8) with CALYPSO at 1 atm, 10 and 20 GPa, with simulation cells containing up to eight B_nN formula units. The predicted *C*222 B_2N (Fig. 1a) and *P*3*m*1 B_3N (Fig. 1b) compounds consist of B atom layers with a cubic and hexagonal BN, respectively, indicating possible unstability with respect decomposition into solid boron and BN. On the other hand, in B_4N, B_6N, and B_8N, all boron atoms form icosahedra. Interestingly, we predicted a high-symmetry cubic $Pm\bar{3}n$ structure for B_4N, with six formula units in each unit cell. In this structure, the centers of boron icosahedra form a body-centered cubic (bcc) lattice with nitrogen atoms partially located at the tetrahedral sites, as shown in Fig. 1c. Each nitrogen atom is bonded to four nearest icosahedra and there is no B–B bond between the icosahedra. If we take each boron icosahedron as a unit, then $Pm\bar{3}n$ B_4N can be seen as the well-known Nb_3Sn-type structure. In $P6_3/mmc$ B_5N, 15 boron atoms form a polyhedron with a B–B bond length of 1.69 Å between different polyhedra and each nitrogen atom is attached to the three closest polyhedra.

For B_6N, we first considered $R\bar{3}m$, *Cmcm* and *Imma* structures, which are taken from other A_6B-type compounds, such as B_6As [14,15], and B_6Si [39] (Fig. S1). In these three structures, each N is attached to three boron icosahedra. To verify the reliability of the current calculations, we compared the bond lengths of $R\bar{3}m$ B_6N with previous theoretical calculation. The calculated bond lengths are 1.688, 1.789, 1.803, 1.806 and 1.818 Å for B–B bonds and 1.479 Å for B–N bonds, which are close to those of 1.670, 1.762, 1.775, 1.779 and 1.789 Å for B–B bonds and 1.464 Å for B–N bonds in previous calculations [6]. Our subsequent structure searches also predict the metastable *Cmcm* phase. However, two more stable *Cmca* and *Immm* structures are predicted, where each N atom is bonded to four boron icosahedra. Increasing the number of bonds between N atoms and boron icosahedra could be the reason for making *Cmca* and *Immm* structures more stable, compared with $R\bar{3}m$, *Cmcm* and *Imma*. The *Cmca* structure is the most stable one for B_6N, which is similar to the one predicted for B_6Si under pressure, which can be obtained from the *Cmca* LiB_6Si by eliminating the Li atoms [40]. Moreover, there are also B–B bonds between different icosahedra in $R\bar{3}m$(1.688 Å), *Cmcm* (1.668, 1.688 Å), *Imma* (1.694, 1.731 Å), *Immm* (1.663 Å) and *Cmca* (1.648 Å), which are shorter than

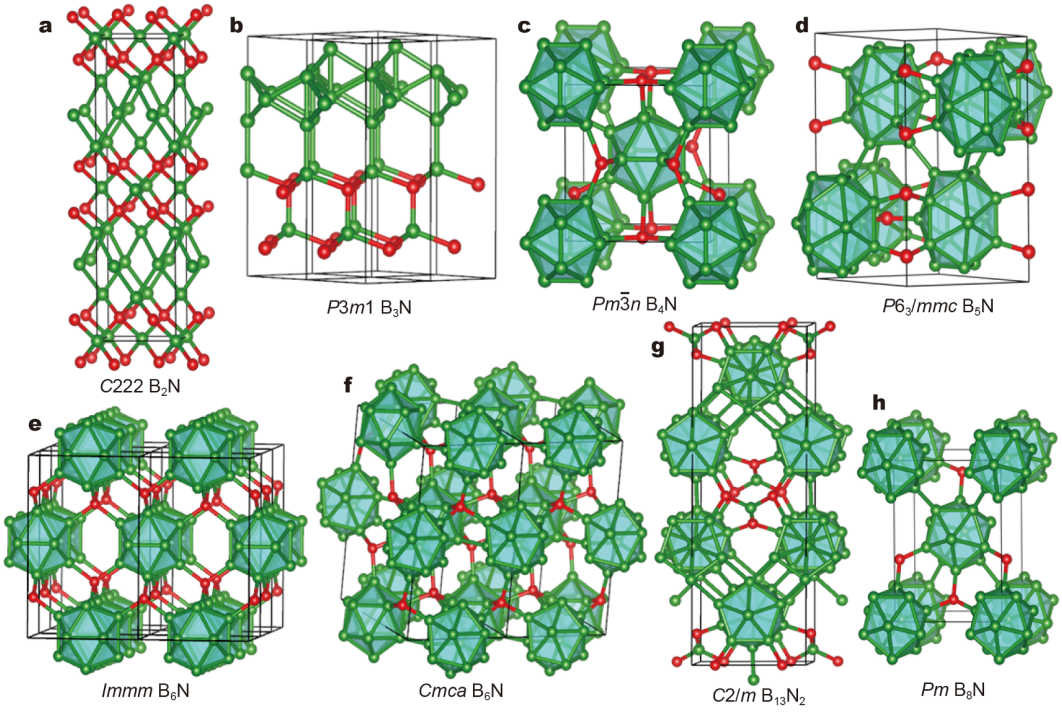

Figure 1 Predicted structures of boron-rich B-N compounds. (a) *C*222 B_2N, (b) *P*3*m*1 B_3N, (c) $Pm\bar{3}n$ B_4N, (d) $P6_3/mmc$ B_5N, (e) *Immm* B_6N, (f) *Cmca* B_6N, (g) *C*2/*m* $B_{13}N_2$, and (h) *Pm* B_8N. Red balls are N and green ones are B.

those B–B bonds in the corresponding icosahedra. For example, they are 1.734, 1.735, 1.756, 1.765, 1.775, 1.805, 1.812, 1.823, 1.877 Å for *Cmca* and 1.729, 1.776, 1.808, 1.819, 1.828, 1.841 Å for *Immm* B_6N.

The predicted most stable structure for B_8N is a monoclinic *Pm* phase, where each N atom is also bonded to three different boron icosahedra. Half of the boron atoms of each icosahedron are also bonded to the boron atoms in the nearest icosahedron, five are bonded to the nearest nitrogen atoms and another one is not bonded, with a much longer B–B distance of 2.233 Å. The bond lengths of B–B between different icosahedra are 1.682, 1.685, 1.687 and 1.69 Å. For $B_{13}N_2$, we predicted a monoclinic *C*2/*m* structure, where N atoms show three or four bonds with B atoms. In addition, as it is shown in Fig. S1, we also predicted metastable *Pma*2 and $I4_1/amd$ B_2N, *Imm*2 B_3N, *P*2/*c* B_4N, *P*6/*mmm* B_5N, $Im\bar{3}m$ B_8N, and *P*6/*mmm* $B_{13}N_2$ structures. Detailed information on the predicted crystal structures is given in Table S1.

Enthalpy ratios for different B_nN stoichiometries at 1 atm and 20 GPa are summarized in Fig. 2 and Fig. S2. The solid symbols on the solid line indicate that those boron nitrides are stable at the corresponding pressures, while those stoichiometries that are not on the line indicate they are unstable with respect to decomposition or disproportionation into other boron nitrides and pure boron or nitrogen. As we can see, at 1 atm all the stoichiometries have negative formation enthalpies, suggesting that they are stable with respect to disproportionation into pure boron and nitrogen. The already known BN stoichiometry has the lowest formation enthalpy. On the nitrogen-rich side, the previously predicted B_3N_5 is calculated to be on the solid line, suggesting that it is also thermodynamically stable without decomposition into h-BN and pure nitrogen [41]. On the boron-rich side, the previously reported $B_{50}N_2$ compounds are thermodynamically stable with respect to h-BN and α-B, which is in good agreement with previous experiments [23]. $B_{38}N_6$ is stable with respect to c-BN and α-B in previous theoretical calculations [25]. However, when the reference level is h-BN, which is the most stable form at 1 atm for BN, $B_{38}N_6$ is metastable with respect to h-BN and α-B. The predicted B_2N, B_3N, B_4N, B_5N and B_8N compounds are all metastable and decompose into h-BN and pure boron. Interestingly, the predicted *Cmca* B_6N is the only new stable structure. Unfortunately, the experimentally proposed $R\bar{3}m$ and the currently predicted *C*2/*m* $B_{13}N_2$ are both calculated to be thermodynamically unstable with respect to $B_{38}N_6$ and α-B, and the calculated phonon spectra (Fig. S3) indicate that $B_{38}N_6$ is dynamically stable.

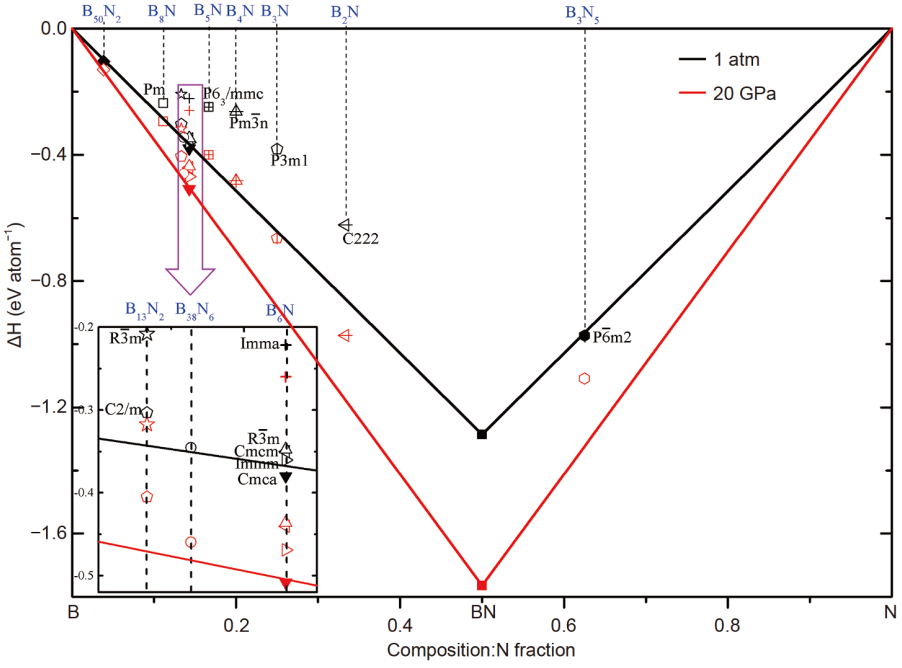

Figure 2 Formation enthalpies per atom of different $B_{1-x}(1/2N_2)_x$ stoichiometries with respect to their constituent counterparts at 1 atm and 20 GPa. Different symbols represent different structures for different stoichiometries and the same symbols with different colors represent different pressures. The reference level is pure boron (α-B or γ-B) and pure nitrogen ($Pa\bar{3}$ or $P4_12_12$), both in their most stable forms at the specified pressures. For BN, we considered h-BN and cubic boron nitride (c-BN) at 1 atm and 20 GPa, respectively.

Moreover, the simulated powder XRD pattern of $B_{38}N_6$ (Fig. S4) is in good agreement with the experimental powder-diffraction data of $B_{13}N_2$ [28] and previous theoretical study [25]. Therefore, the observed $R\bar{3}m$ $B_{13}N_2$ is more likely to be the proposed $B_{38}N_6$. This result is the same as in the Ref. [25], and the consistency between the calculated and measured Vickers hardness further support this opinion. The formation enthalpies of all the structures at 20 GPa become more negative, while B_6N and BN are still on the solid line, suggesting that they are thermodynamically stable even under pressure.

After analyzing the thermodynamical stability of boron-rich nitrides, we have also checked their dynamical stability. Phonon calculations were performed using the supercell approach method within the PHONOPY code [42] to determine the dynamic stability. Except $R\bar{3}m$ $B_{13}N_2$, the calculated phonon dispersion curves for various stoichiometries do not have imaginary frequencies, indicating that they are all dynamically stable both at 1 atm and under pressure (Figs S3 and S5).

To study the electronic properties of the predicted B-N compounds, their electronic band structures were calculated, as shown in Fig. 3, Figs S6 and S7. The atomic contributions to the bands are also displayed to explore their origins. It is clear that *C*222 B_2N, $Pm\bar{3}n$ B_4N, *Cmcm* B_6N and *Pm* B_8N are metallic, with bands crossing the Fermi level (E_f), while *Cmca* and *Immm* B_6N are semiconductors with direct and indirect band gaps of 2.45 and 3.01 eV, respectively. In *C*222 B_2N (Fig. 3a) the electronic states around E_f are mainly associated to B atoms in B–B bonds. Interestingly, the valences and conduction bands near the E_f exhibit a linear dispersion with two crossing points along the *Γ*-*Z* and *T*-*Y* directions. As shown in Fig. S8a, the density of states at E_f is almost zero, revealing that *C*222 B_2N is a semimetal. Moreover, the energy of the highest valence and lowest conduction bands are inverted along the *Z*-*T* direction. These features indicate that *C*222 B_2N could be a topological semimetal. In $Pm\bar{3}n$ B_4N, all the B atoms are equivalent and only bonded to N atoms, without forming B–B bonds between different icosahedra. As shown in Fig. 3b, the electronic states near the E_f mainly come from the equivalent B atoms. To explore the superconductivity of B_4N, its superconducting transition temperature T_c is also estimated with the Allen-Dynes modified McMillan equation:

$$T_c = \frac{\omega_{\log}}{1.2}\exp\left[-\frac{1.04(1+\lambda)}{\lambda-\mu^*(1+0.62\lambda)}\right].$$

The electron-phonon coupling (EPC) calculations were performed within the density functional perturbation theory, as implemented in the Quantum ESPRESSO package [43], where ultrasoft pseudopotentials for B and N were considered with a kinetic energy cutoff of 50 Ry. 3×3×3 *q*-meshes in the first Brillouin zones were used in the EPC calculations. The calculated logarithmic average frequency, $\omega_{\log}$, is 938 K and the EPC parameter, λ, is 0.31. With a typical choice of the Coulomb pseudopotential μ^* of 0.1, the calculated T_c is only 0.59 K, indicating that $Pm\bar{3}n$ B_4N is not a good superconductor (Fig. S9).

In the semiconducting *Cmca* and *Immm* B_6N (Fig. 3c, d), the highest occupied valence bands are mainly associated to the B_{12} icosahedra, especially to those B atoms that form bonds with other Bs only. Compared with *Cmca* and *Immm* B_6N, the partially occupied bands crossing the E_f for $P6_3/mmc$ B_5N, $R\bar{3}m$, *Cmcm* and *Immm* B_6N, and *Pm* B_8N are mainly related to N atoms, inducing the metallic character.

As boron-rich compounds are often potential candidates for superhard materials, we also studied the mechanical properties of the predicted boron-rich nitrides. Table 1 and Table S2 list the calculated bulk modulus, shear modulus and Vickers hardness of the predicted boron-rich nitrides. According to the semiempirical hardness model for covalent crystals by Gao *et al.* [44–47], the calculated Vickers hardness for $R\bar{3}m$ and *C*2/*m* $B_{13}N_2$ are 37.4 and 37.3 GPa, respectively, while it is 39.9 GPa for *C*2/*m* $B_{38}N_6$, which is much closer to the experimentally measured value of 41 GPa [22]. The calculated hardness further supports that the proposed *C*2/*m* $B_{38}N_6$ is more likely to be the experimentally synthesized "$B_{13}N_2$". Additionally, the Vickers hardness of B_4N, B_6N and B_8N are also estimated to be 45, 38−42 and 39 GPa, respectively. The calculated Vickers hardness of $Pm\bar{3}n$ B_4N as well as *Cmca* and *Immm* B_6N are all 40 GPa, suggesting that they are potential superhard materials. Among these boron-rich compounds, there are three types of bonds: B–N bonds, B–B bonds within B_{12} icosahedra, and B–B bonds outside B_{12} icosahedra. For more than 70% of the bonds are coming from B–B bonds within icosahedra in these B_nN compounds, the hardness are mainly contributed from B_{12} icosahedra. In addition, a B–N bond usually contributes more to hardness than a B–B bond, therefore, the increase of B–N bonds will improve hardness. In B_4N, each nitrogen atom is bonded to four nearest icosahedra, and B_{12} icosahedra are only connected with N atoms, forming short B–N bonds. In B_6N and B_8N, the B_{12} icosahedra are also connected with adjacent icosahedra, forming long B–B bonds. Moreover, in *Cmcm*, $R\bar{3}m$ B_6N and *Pm* B_8N, each nitrogen atom is

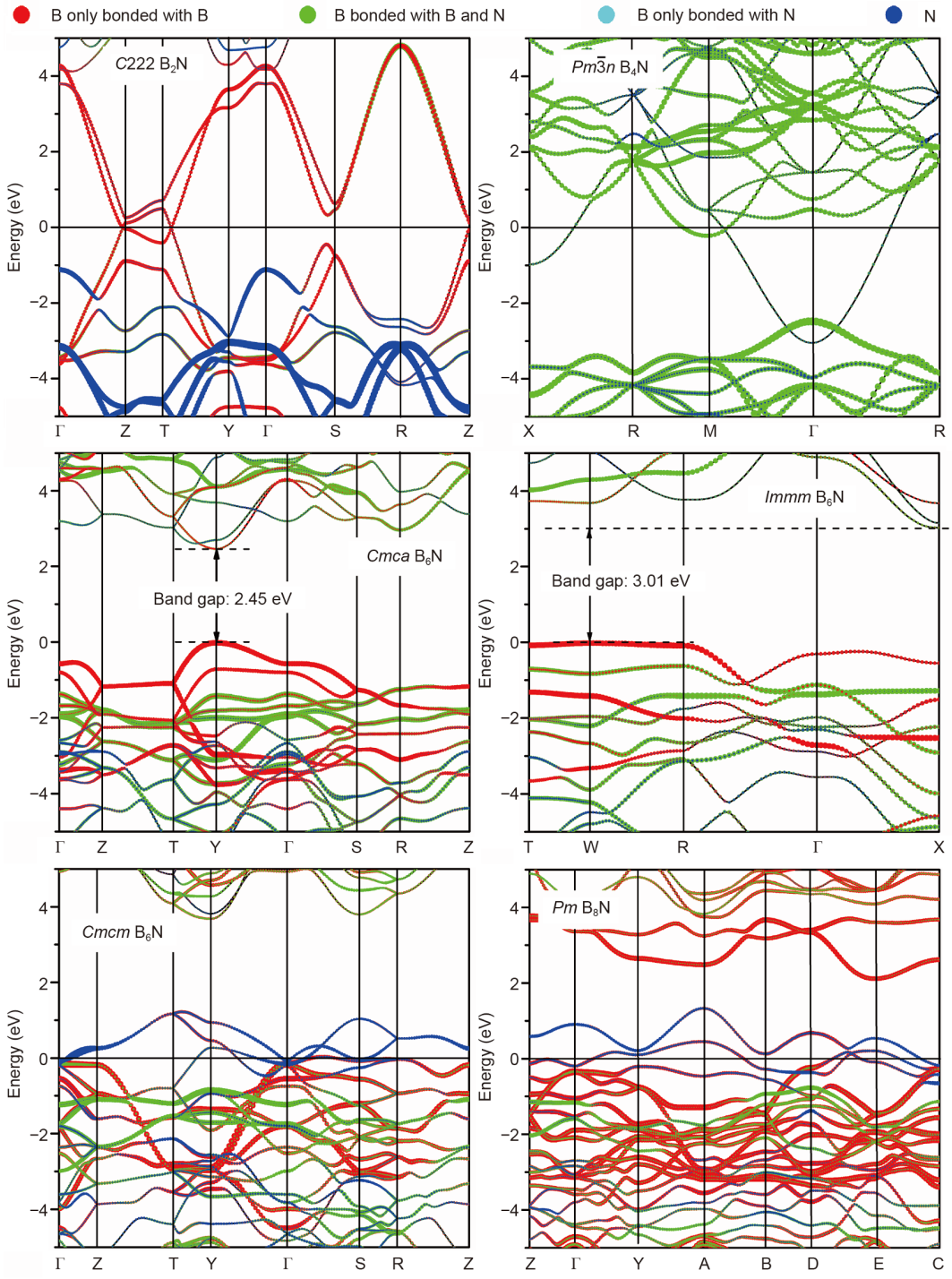

Figure 3 The calculated electronic band structures for (a) *C*222 B_2N, (b) *Pm*$\bar{3}$*n* B_4N, (c) *Cmca* B_6N, (d) *Immm* B_6N, (e) *Cmcm* B_6N, and (f) *Pm* B_8N at 1 atm.

only bonded to three nearest icosahedra, which results in the decrease of B–N bonds. Therefore, B_4N shows a higher hardness than B_6N and B_8N.

In addition, Vickers hardness can also be estimated using the model of Chen *et al.* [48] with the following expression $H_v(\text{GPa})=2(G^3/B^2)^{0.585}-3$, where G and B are the shear and bulk moduli, respectively (Table S2). With this approximation, the Vickers hardness of B_4N is esti-

Table 1 The calculated Vickers Hardness (H_v, GPa) of the boron-rich nitrides

Crystal	H_v (GPa)[a]
$Pm\bar{3}n$ B_4N	44.6
$Cmca$ B_6N	41.9
$Immm$ B_6N	41.6
$Cmcm$ B_6N	38.5
$R\bar{3}m$ B_6N	38.7
$R\bar{3}m$ $B_{13}N_2$	37.4
$C2/m$ $B_{13}N_2$	37.3
$C2/m$ $B_{38}N_6$	39.9
Pm B_8N	39.1
$Im\bar{3}m$ B_8N	38.9

a) From Gao *et al.*'s [44–47] model.

mated to be 45.4 GPa, which is also in agreement with the value obtained with the model of Gao *et al.* [44–47]. The calculated hardness of the other stoichiometries are almost similar to those of the model of Gao *et al.* [44–47], except in *Cmca* B_6N and $R\bar{3}m$ $B_{13}N_2$, where they show larger differences. The calculated elastic constants for *Cmca*, *Immm*, *Cmcm* and $R\bar{3}m$ B_6N, $Pm\bar{3}n$ B_4N, *Pm* and $Im\bar{3}m$ B_8N, as well as *C*2/*m*, $R\bar{3}m$ $B_{13}N_2$, and *C*2/*m* $B_{38}N_6$ satisfy the corresponding mechanical stability criteria, suggesting that they are mechanically stable (Table S3).

In summary, different stoichiometries and their crystal structures of boron-rich nitrides under pressure have been extensively explored. In B_nN ($n\geq4$) stoichiometries, except in B_5N, all boron atoms are capable of forming icosahedra. $B_{50}N_2$ is calculated to be stable at 1 atm, which is in agreement with the experiments. Three new orthorhombic structures are predicted for B_6N and cubic and monoclinic phases for B_4N and B_8N, respectively. B_6N is also predicted to be stable below 20 GPa and B_4N and B_8N are metastable, although BN always has the lowest enthalpy. Two structures for B_6N are semiconductors and the other stoichiometries are all metallic. Moreover, the stable B_6N and metastable B_4N are estimated to be potential superhard materials, and B_4N is also estimated to be superconductor with a very low T_c value of 0.59 K. The current study will enrich the phase diagram of the B-N system and may also stimulate the experimental work in the future.

Received 5 March 2020; accepted 7 May 2020; published online 9 July 2020

1 Thévenot F. Boron carbide—A comprehensive review. J Eur Ceramic Soc, 1990, 6: 205–225
2 Albert B, Hillebrecht H. Boron: Elementary challenge for experimenters and theoreticians. Angew Chem Int Ed, 2009, 48: 8640–8668
3 Pan Y, Zhou B. ZrB2: Adjusting the phase structure to improve the brittle fracture and electronic properties. Ceram Int, 2017, 43: 8763–8768
4 Pan Y, Lin Y. Influence of B concentration on the structural stability and mechanical properties of Nb–B compounds. J Phys Chem C, 2015, 119: 23175–23183
5 Gao F, Hou L, He Y. Origin of superhardness in icosahedral B_{12} materials. J Phys Chem B, 2004, 108: 13069–13073
6 Guo X, He J, Liu Z, *et al.* Bond ionicities and hardness of $B_{13}C_2$-like structured B_yX crystals (X=C, N, O, P, As). Phys Rev B, 2006, 73: 104115
7 Veprek S, Zhang RF, Argon AS. Mechanical properties and hardness of boron and boron-rich solids. J Superhard Mater, 2011, 33: 409–420
8 Will G, Kossobutzki KH. An X-ray structure analysis of boron carbide, $B_{13}C_2$. J Less Common Met, 1976, 44: 87–97
9 Morosin B, Aselage T, Emin D. On the crystal structure of boron carbides. AIP Conf Proc, 1991, 231: 193–196
10 An Q, Goddard WA. Atomistic origin of brittle failure of boron carbide from large-scale reactive dynamics simulations: Suggestions toward improved ductility. Phys Rev Lett, 2015, 115: 105501
11 Olofsson M, Lundström T. Synthesis and structure of non-stoichiometric B_6O. J Alloys Compd, 1997, 257: 91–95
12 Peret JL. Preparation and properties of the boron phosphides. J Am Ceramic Soc, 1964, 47: 44–46
13 Yang P, Aselage TL. Synthesis and cell refinement for icosahedral boron phosphide $B_{12}P_2$. Powder Diffr, 1995, 10: 263–265
14 Morrison I, Bylander DM, Kleinman L. Bands and bonds of $B_{12}As_2$. Phys Rev B, 1992, 45: 1533–1537
15 Bakalova S, Gong Y, Cobet C, *et al.* Electronic excitations in $B_{12}As_2$ and their temperature dependence by vacuum ultraviolet ellipsometry. J Phys-Condens Matter, 2010, 22: 395801
16 Condon JB, Holcombe CE, Johnson DH, *et al.* The kinetics of the boron plus nitrogen reaction. Inorg Chem, 1976, 15: 2173–2179
17 Hubert H, Garvie LAJ, Buseck PR, *et al.* High-pressure, high-temperature syntheses in the B–C–N–O system. J Solid State Chem, 1997, 133: 356–364
18 Solozhenko VL, Le Godec Y, Kurakevych OO. Solid-state synthesis of boron subnitride, B_6N: myth or reality? Comptes Rendus Chimie, 2006, 9: 1472–1475
19 Saitoh H, Yoshida K, Yarbrough WA. Crystal structure of new composition boron-rich boron nitride using raman spectroscopy. J Mater Res, 1993, 8: 8–11
20 Kurakevych OO, Solozhenko VL. Rhombohedral boron subnitride, $B_{13}N_2$, by X-ray powder diffraction. Acta Crystlogr C Cryst Struct Commun, 2007, 63: i80–i82
21 Solozhenko VL, Kurakevych OO. New boron subnitride $B_{13}N_2$: HP-HT synthesis, structure and equation of state. J Phys-Conf Ser, 2008, 121: 062001
22 Solozhenko VL, Bushlya V. Mechanical properties of superhard boron subnitride $B_{13}N_2$. J Superhard Mater, 2017, 39: 422–426
23 Solozhenko VL, Turkevich VZ. Phase diagram of the B–BN system at pressures up to 24 GPa: Experimental study and thermodynamic analysis. J Phys Chem C, 2018, 122: 8505–8509
24 Zhang H, Yao S, Widom M. Predicted phase diagram of boron-carbon-nitrogen. Phys Rev B, 2016, 93: 144107
25 Ektarawong A, Simak SI, Alling B. Thermodynamic stability and properties of boron subnitrides from first principles. Phys Rev B, 2017, 95: 064206

26 Ploog K, Schmidt H, Amberger E, *et al.* $B_{48}B_2C_2$ und $B_{48}B_2N_2$, zwei nichtmetallboride mit der struktur des sog. I tetragonalen bors. J Less Common Met, 1972, 29: 161–169
27 Will G, Kossobutzki KH. X-ray diffraction analysis of $B_{50}C_2$ and $B_{50}N_2$ crystal-lizing in the "tetragonal" boron lattice. J Less Common Met, 1976, 47: 33–38
28 Solozhenko VL, Kurakevych OO. Chemical interaction in the B–BN system at high pressures and temperatures.. J Solid State Chem, 2009, 182: 1359–1364
29 Cherednichenko KA, Solozhenko VL. Structure and equation of state of tetragonal boron subnitride $B_{50}N_2$. J Appl Phys, 2017, 122: 155901
30 Wang Y, Lv J, Zhu L, *et al.* Crystal structure prediction *via* particle-swarm optimization. Phys Rev B, 2010, 82: 094116
31 Lv J, Wang Y, Zhu L, *et al.* Predicted novel high-pressure phases of lithium. Phys Rev Lett, 2011, 106: 015503
32 Zhu L, Wang H, Wang Y, *et al.* Substitutional alloy of Bi and Te at high pressure. Phys Rev Lett, 2011, 106: 145501
33 Wang Y, Lv J, Zhu L, *et al.* CALYPSO: A method for crystal structure prediction. Comput Phys Commun, 2012, 183: 2063–2070
34 Liang X, Bergara A, Wang L, *et al.* Potential high-T_c superconductivity in $CaYH_{12}$ under pressure. Phys Rev B, 2019, 99: 100505
35 Wang L, Tian F, Liang X, *et al.* High-pressure phases of boron arsenide with potential high thermal conductivity. Phys Rev B, 2019, 99: 174104
36 Kresse G, Furthmüller J. Efficient iterative schemes for *ab initio* total-energy calculations using a plane-wave basis set. Phys Rev B, 1996, 54: 11169–11186
37 Perdew JP, Chevary JA, Vosko SH, *et al.* Atoms, molecules, solids, and surfaces: applications of the generalized gradient approximation for exchange and correlation. Phys Rev B, 1992, 46: 6671–6687
38 Kresse G, Joubert D. From ultrasoft pseudopotentials to the projector augmented-wave method. Phys Rev B, 1999, 59: 1758–1775
39 Liang X, Bergara A, Xie Y, *et al.* Prediction of superconductivity in pressure-induced new silicon boride phases. Phys Rev B, 2020, 101: 014112
40 Vojteer N, Schroeder M, Röhr C, *et al.* $Li_2B_{12}Si_2$: The first ternary compound in the system Li/B/Si: Synthesis, crystal structure, hardness, spectroscopic investigations, and electronic structure. Chem Eur J, 2008, 14: 7331–7342
41 Li Y, Hao J, Liu H, *et al.* High-energy density and superhard nitrogen-rich B-N compounds. Phys Rev Lett, 2015, 115: 105502
42 Togo A, Oba F, Tanaka I. First-principles calculations of the ferroelastic transition between rutile-type and $CaCl_2$-type SiO_2 at high pressures. Phys Rev B, 2008, 78: 134106
43 Giannozzi P, Baroni S, Bonini N, *et al.* QUANTUM ESPRESSO: a modular and open-source software project for quantum simulations of materials. J Phys-Condens Matter, 2009, 21: 395502
44 Gao F, He J, Wu E, *et al.* Hardness of covalent crystals. Phys Rev Lett, 2003, 91: 015502
45 Tian Y, Xu B, Zhao Z. Microscopic theory of hardness and design of novel superhard crystals. Int J Refractory Met Hard Mater, 2012, 33: 93–106
46 Xu B, Tian Y. Superhard materials: recent research progress and prospects. Sci China Mater, 2015, 58: 132–142
47 Hu W, Wen B, Huang Q, *et al.* Role of plastic deformation in tailoring ultrafine microstructure in nanotwinned diamond for enhanced hardness. Sci China Mater, 2017, 60: 178–185
48 Chen XQ, Niu H, Li D, *et al.* Modeling hardness of polycrystalline materials and bulk metallic glasses. Intermetallics, 2011, 19: 1275–1281

Acknowledgements This work was supported by the Fostering Program of Major Research Plan of the National Natural Science Foundation of China (91963115), the National Key R&D Program of China (2018YFA0703400), the National Natural Science Foundation of China (51732010), and the PhD Foundation by Yanshan University (B970). Bergara A acknowledges financial support from the Spanish Ministry of Economy and Competitiveness (FIS2016-76617-P) and the Department of Education, Universities and Research of the Basque Government and the University of the Basque Country (IT756-13).

Author contributions Gao G conceived the project and wrote the paper. Wang L, Sun R, Liu W, Liang X and Yuan Z performed the calculations. All the authors analyzed the data, discussed the results and commented on the manuscript.

Conflict of interest The authors declare that they have no conflict of interest.

Supplementary information Experimental details and supporting data are available in the online version of the paper.

Linyan Wang is a PhD candidate at the College of Materials Science and Engineering, Yanshan University. Her research interest focuses on theoretical design and experimental synthesis of novel metastable materials under high pressure and high temperature.

Guoying Gao is a professor at the College of Materials Science and Engineering, Yanshan University. She received her PhD degree from Jilin University in 2011. Her research interest focuses on theoretical design and experimental synthesis of novel metastable materials under high pressure and high temperature.

高压下新型超硬富硼氮化物

王林妍[1†], 孙荣鑫[1†], 刘雯慧[1†], 袁智康[1†], Aitor Bergara[2,3,4], 梁笑微[1], 陈帅[1], 周向锋[1], 徐波[1], 何巨龙[1], 于栋利[1], 高国英[1*], 田永君[1]

摘要 富硼化合物通常为潜在的超硬材料, 尽管之前的研究提出了不同晶型的BN超硬材料, 但尚未发现超硬的富硼氮化物. 本文采用基于粒子群优化算法的结构预测方法, 结合第一性原理计算, 对富硼氮化物在压力下的稳定成分及结构进行系统研究. 结果表明, 在B_4N、B_6N和B_8N中, 硼原子都能够形成B_{12}二十面体. 在0–20 GPa压力范围内, B_6N是热力学稳定的, 而B_4N和B_8N是亚稳的. 电子性质计算表明, 预测的*Cmca* B_6N和*Immm* B_6N为半导体, 其他均为金属. 声子和弹性常数计算表明, 所有预测结构都具有动力学稳定性和机械稳定性. 值得关注的是, B_4N和B_6N的维氏硬度分别为45和42 GPa, 表明其为潜在的超硬材料. 此研究丰富了B-N体系相图, 并为实验上探索超硬材料提供了丰富的理论指导.

